Inorganic Chemistry

Article

pubs.acs.org/IC

Spin Crossover, Reversible Redox, and Supramolecular Interactions in 3d Complexes of 4-(4-Pyridyl)-2,5-dipyrazyl-pyridine

Reece G. Miller and Sally Brooker*

Department of Chemistry and the MacDiarmid Institute for Advanced Materials and Nanotechnology, University of Otago, P.O. Box 56, Dunedin 9054, New Zealand

Supporting Information

ABSTRACT: A new terpyridine-inspired terdentate ligand, 4-(4-pyridyl)-2,5-dipyrazyl-pyridine (**py-pzpypz**), featuring three "spare" nitrogen donors "out the back", has been used to synthesize five bis-ligand complexes, $[M^{II}(\mathbf{py\text{-}pzpypz})_2]X_2$, where M = Mn with X = ClO_4, or M = Fe, Co, Ni, and Zn with X = BF_4. In contrast, when M = Cu^{II}, regardless of the M:L ratio employed, 1:1 M:L products were obtained: for X = BF_4 a 1D chain $\{[Cu^{II}(\mathbf{py\text{-}pzpypz})(DMF)_2](BF_4)_2\}_n$, and for X = Cl a monometallic complex $[Cu(\mathbf{py\text{-}pzpypz})Cl_2]$. All seven complexes were structurally characterized, confirming the expected N_6 coordination of the M^{II} centers in all cases except Cu^{II}. Notably, a Jahn–Teller elongation is observed in the Co^{II} complex, consistent with it being low spin at 100 K. The Cu^{II} 1D chain complex has an N_4O_2 coordination sphere as in this case the "spare" pyridine donor out the back of the **py-pzpypz** ligand bridges to the next Cu^{II} center in the chain, hence providing both a terdentate site and a monodentate pyridine to the next Cu^{II} center, and the coordination sphere is completed by weak axial coordination by two DMF solvent molecules. The Cu^{II} center in the monometallic complex has an N_3Cl_2 square pyramidal coordination sphere. In all cases, the noncoordinating, "spare", pyrazine nitrogen atoms are involved in interesting intermolecular interactions, including N_{Pz}–π interactions and nonclassical C–H···N_{Pz} hydrogen bonding. The Fe^{II} complex is low spin as expected. Two polymorphs of the Co^{II} complex were obtained, both of which showed gradual spin crossover, with a room temperature $T_{1/2}$. Two reversible redox processes are observed for $[Co^{II}(\mathbf{py\text{-}pzpypz})_2](BF_4)_2$, with $E_m(M^I/M^{II})$ = −0.63 V and $E_m(M^{II}/M^{III})$ = +0.37 V, and a quasireversible redox process for $[Fe^{II}(\mathbf{py\text{-}pzpypz})_2](BF_4)_2$, with $E_m(M^{II}/M^{III})$ = +1.26 V, versus 0.01 M $AgNO_3$/Ag in MeCN. These potentials are shifted to significantly higher potentials (by ∼0.45 V) than the literature values for the corresponding Fe^{II} and Co^{II} complexes of the equivalent all-pyridine ligand, consistent with replacement of the two pyridine rings by two pyrazine rings significantly stabilizing the lower oxidation states.

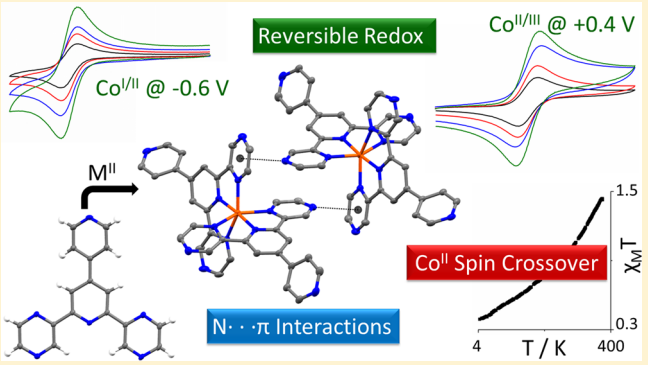

INTRODUCTION

Terpyridine (**L1**, Figure 1) was first prepared in 1932,[1] but only after more user-friendly syntheses were developed[2−4] did the chemistry of terpyridines accelerate, from a solid baseline of activity to publication rates growing almost exponentially since the 1990s.[5] Transition metal complexes of terpyridine and related 4-substituted derivatives have been widely studied due to their interesting magnetic, optical, electrochemical, catalytic, and DNA binding properties.[5−20] Focusing in further, to 3d complexes, spin crossover (SCO) in cobalt(II) complexes of terpyridine and its derivatives is well-known,[14,21−25] and in all but a few cases[14,24] these are gradual and without a thermal hysteresis.[14,21−25] Other examples of cobalt(II) complexes of terpyridine derivatives (e.g., **L5**, Figure 1) have shown interesting photochemical properties such as photocleavage of DNA.[11] Ligands, like **L5**, which feature an additional donor within the 4-substituent "off the back" of the terpy moiety have also been used to explore the controlled formation of interesting supramolecular architectures.[5,13,15] Iron(II) complexes of terpyridine-like ligands are almost always low spin at room temperature[26] (unless sterically hindered[27,28]) but often show interesting reversible redox behavior.[29−31]

The pyrazine analogues of these terpyridine-type ligands have received far less attention (e.g., **L2**–**L4**, Figure 1),[32,33] with the replacement of one or more pyridine rings by pyrazine rings first reported by Plé and co-workers in 2005.[32] These new pyrazine analogues are of interest to coordination chemists for two main reasons.

First, the electronics are changed due to the weaker σ-donor and stronger π-acceptor nature of pyrazine[34] which is generally expected to stabilize the low spin (LS) state[34−41] and to increase the M^{II}/M^{III} potential of the complex, relative to that of the pyridine analogue.[33,38,40] With regard to the former expectation, intriguingly Halcrow and co-workers showed that replacing only the central pyridine of terpyridine (**L1**) by

Received: February 24, 2015
Published: May 13, 2015

DOI: 10.1021/acs.inorgchem.5b00428
Inorg. Chem. 2015, 54, 5398−5409

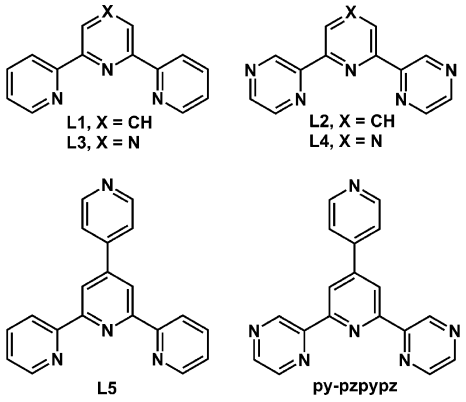

Figure 1. Terpyridine **L1**, 2,6-di(pyrazinyl)pyridine **L2**,[32] 2,6-di(pyrid-2-yl)pyrazine **L3**,[32] terpyrazine **L4**,[32] 4-(4-pyridyl)-2,5-terpyridine **L5**,[29] and 4-(4-pyridyl)-2,5-dipyrazyl-pyridine **py-pzpypz** (this work).

pyrazine, giving **L3**, resulted in essentially high spin (HS) complexes, $[Co^{II}(\mathbf{L3})_2](BF_4)_2$, whereas replacing either the two distal pyridine rings, giving **L2**, or all three pyridine rings, giving **L4**, resulted in predominantly low spin (LS) complexes, $[Co^{II}(\mathbf{Ln})_2](BF_4)_2$ with n = 2 or 4.[33] In contrast, as expected, they observed an increase in M^{II}/M^{III} potential (vs Fc/Fc^+ in MeCN) on replacing pyridine rings by pyrazine rings: whereas the $E_{1/2}(Fe^{II}/Fe^{III})$ for $[Fe^{II}(\mathbf{L1})_2](BF_4)_2$ was +0.71 V, for the pyrazine **L2**−**L4** analogues it was +0.95 to +1.36 V. Likewise, the $E_{1/2}(Co^{II}/Co^{III})$ for $[Co^{II}(\mathbf{L1})_2](BF_4)_2$ was −0.13 V whereas for the **L2**−**L4** analogues it was between +0.12 and +0.49 V.

Second, replacement of one or more pyridine rings by pyrazine rings in these ligands results in "spare" nitrogen donors "out the back" of the ligand. This opens up the possibility of bridging to other metal centers and forming supramolecular arrays, something we have recently reported for some pyrazine imide ligands.[39,40,42,43] Such assemblies are of considerable current interest for their applications in areas such as magnetism,[44,45] gas adsorption,[43,44] and heterogeneous catalysis.[37,46]

Here we report the two-step synthesis of a new 2,6-dipyrazyl-pyridine ligand (Figure 1, Scheme 1, **py-pzpypz**) and the mid-to-late first row transition metal complexes of it (Mn^{II} to Zn^{II}).

Scheme 1. Synthetic Route to the New Ligand py-pzpypz and to the 2:1 M^{II} Complexes of It Reported in This Work

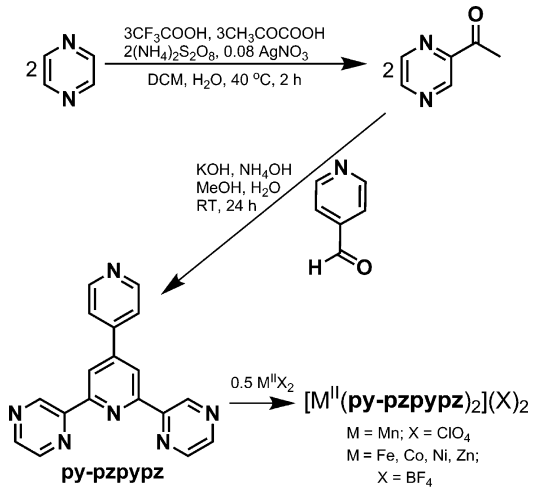

The structures and physical properties of these new complexes are described and compared to those of the better known terpyridine based analogues (Figure 1).

RESULTS AND DISCUSSION

Ligand Synthesis. The new ligand 4-(4-pyridyl)-2,5-dipyrazyl-pyridine (**py-pzpypz**) was synthesized in two straightforward steps from the commercially available reagents pyrazine and pyridine-4-carbaldehyde (Scheme 1).

First, 2-acetylpyrazine was prepared in 45% yield from pyrazine, by the method previously reported by Minisci and co-workers.[47] Then it was reacted with 0.5 equiv of pyridine-4-carbaldehyde using a method adapted from that reported by Constable and Thompson for **L5**.[29] Rather than this being carried out in two separate steps as for **L5**, i.e., initially isolating the diketone (afforded by the 2:1 aldol condensation of 2-acetylpyrazine and pyridine-4-carbaldehyde with NaOH in $EtOH/H_2O$), then cyclizing with NH_4OAc in EtOH, it was found that for **py-pzpypz** the reaction could be carried out in one pot. This was achieved by simply stirring the reagents with NH_4OH and KOH in $MeOH/H_2O$, monitoring the reaction by ^1H NMR spectroscopy. The reaction is complete within 24 h. Then more water is added and the product extracted into $CHCl_3$ which is taken to dryness to give **py-pzpypz** as a pale yellow powder. As **py-pzpypz** has low solubility in acetone, any traces of the starting materials are easily removed with an acetone wash, to give analytically pure **py-pzpypz**, as a white powder in 59% yield.

Synthesis of $[M^{II}(\mathbf{py\text{-}pzpypz})](X)_2$. Analytically pure powder samples of three of the $[M^{II}(\mathbf{py\text{-}pzpypz})_2](X)_2$ complexes, where M = Fe, Co, Zn and X = BF_4, were precipitated immediately on adding a MeOH solution of $M^{II}(BF_4)_2$ to a $MeOH/CHCl_3$ solution of **py-pzpypz**, due to the low solubility of the complexes in this solvent mixture. This method could also be used to prepare the yellow Mn^{II} (X = ClO_4) complex; however, better yields (50%) were obtained using the refluxing MeCN strategy adopted for Ni^{II} (see next paragraph). These Fe^{II} (dark purple), Co^{II} (red), and Zn^{II} (white) complexes are obtained in 48−81% yields. They are insoluble in most common solvents (H_2O, MeOH, $CHCl_3$, DCM), with the notable exception of MeCN.

When this rapid precipitation from $MeOH/CHCl_3$ method was attempted for Ni^{II} with X = BF_4, an *impure* yellow solid, that is not soluble in any of the above solvents, or in MeCN at room temperature (RT), formed. Therefore, an MeCN suspension of this impure yellow powder was refluxed until it became a golden solution. It remained a solution on cooling, so diethyl ether was vapor diffused into it, resulting in golden block shaped crystals of the desired octahedral complex $[Ni^{II}(\mathbf{py\text{-}pzpypz})_2](BF_4)_2$. However, the yield is improved, and the synthesis simplified, by simply carrying out the reaction in boiling MeCN. Subsequent $CHCl_3$ vapor diffusion into the concentrated MeCN reaction solution gives golden block crystals of $[Ni^{II}(\mathbf{py\text{-}pzpypz})_2](BF_4)_2$ in 67% yield.

Similarly, when the 1:2 M:L reaction was attempted for Cu^{II}, specifically with copper(II) tetrafluoroborate, in $MeOH/CHCl_3$, an *impure* green solid rapidly precipitated. Subsequent recrystallization of this solid, by dissolution in DMF and then vapor diffusion of Et_2O, resulted in green block shaped crystals of the 1D chain complex $\{[Cu(\mathbf{py\text{-}pzpypz})(DMF)_2](BF_4)_2\}_n$. Despite the 1:2 Cu:L reaction, the product is 1:1. It is not uncommon for Cu^{II} to prefer $CuLX_2$ and 5-coordination, over CuL_2 and 6-coordination, when L is a relatively rigid terdentate

DOI: 10.1021/acs.inorgchem.5b00428
Inorg. Chem. 2015, 54, 5398−5409

ligand (X = solvent or anion).[38,40,48,49] Not surprisingly, this 1D chain could be deliberately made, in a better yield (46%) and more simply, by a 1:1 reaction of **py-pzpypz** and $[Cu(H_2O)_6](BF_4)_2$ in DMF at RT, followed by vapor diffusion of Et_2O into the reaction solution. Surprisingly, the 1:1 M:L reaction of copper(II) nitrate and **py-pzpypz** under solvothermal conditions did not produce an analogous 1D chain but rather a mixture containing a few single crystals of mononuclear [Cu(**py-pzpypz**)Cl_2]. This complex could be deliberately prepared in good yield (75%) by carefully layering a solution of copper chloride in methanol on a solution of **py-pzpypz** in a DCM/MeOH mixture.

NMR Spectroscopy. The two diamagnetic complexes, $[M^{II}(\textbf{py-pzpypz})_2](BF_4)_2$ with M = Fe and Zn, were also characterized by ^{1}H NMR spectroscopy and the proton chemical shifts compared to those of the free ligand (Figure 2 and Supporting Information Figure S3).

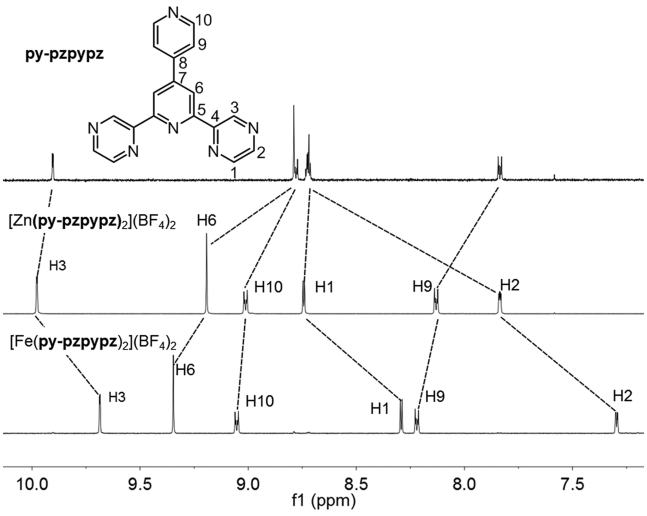

Figure 2. ^{1}H NMR spectra, in d_3MeCN at 400 MHz, of (top to bottom) **py-pzpypz** and Zn^{II} and Fe^{II} complexes. Note: **py-pzpypz** has low solubility in this solvent.

The H3 proton, *meta* to the coordinated pyrazine nitrogen, is shifted slightly downfield in the zinc(II) complex (+0.07 ppm), but upfield in the iron(II) complex (−0.29 ppm), relative to the free ligand. The H2 proton, also *meta* to the coordinated pyrazine nitrogen, but pointing toward the outside of the complex, is shifted strongly upfield in both complexes, but more so in the iron(II) complex (−1.42 ppm) than in the zinc(II) complex (−0.88 ppm). The H1 proton, *ortho* to the coordinated pyrazine nitrogen atom, was almost unaffected by coordination to zinc(II) but shifted significantly upfield in the iron(II) complex (−0.43 ppm). These shifts are all consistent with stronger π-acceptor character[50,51] in the bond between pyrazine and low spin iron(II) than is the case for d^{10} zinc(II).

Structural Characterization. All seven complexes were structurally characterized, and the key structural information is summarized in Tables 1−3. Single crystals of the free ligand, as a hydrochloride salt (Supporting Information Figure S6), were grown by diffusion of HCl(g) (from a 0.1 mol L^{-1} aqueous HCl solution) into a $CHCl_3$ solution of **py-pzpypz** (Supporting Information Table S3 and Figure S6). The protonation occurs at the monodentate pyridine site; a peak corresponding to this proton was present in the residual electron density map. This proton is involved in a strong hydrogen bond to the Cl^- anion [N(6)−H···Cl(1) 3.022(2) Å, 169.5(1)°], providing further confirmation that it is present.

Single crystals of two polymorphs of $[Co(\textbf{py-pzpypz})_2](BF_4)_2$ could be grown, by vapor diffusion of either Et_2O or $CHCl_3$, into an MeCN solution of the complex. When $CHCl_3$ was used as the antisolvent, crystals of the mixed solvate $[Co(\textbf{py-pzpypz})_2](BF_4)_2\cdot MeCN\cdot CHCl_3$ were obtained in the triclinic space group $P\bar{1}$ (polymorph **1**, Figure 3), whereas when Et_2O was used crystals of the solvent-free $[Co(\textbf{py-pzpypz})_2](BF_4)_2$ were obtained in the monoclinic space group $P2_1/n$ (polymorph **2**, Figure 4).

In both polymorphs, at 100 K, the N_6-coordinated cobalt(II) center shows a clear Jahn−Teller distortion, with four short equatorial bonds, and two long axial Co−Npz bonds *within* one of the two terdentate ligands, consistent with the cobalt(II) center being in the *low spin state* (average Co−Npz; ligand 1 = 2.156 Å vs ligand 2 = 1.987 Å). As is usual for terpyridine-type complexes (Table 1), the two Co−N bonds to the central pyridine nitrogen donor of each of the terdentate **py-pzpypz** ligands are significantly shorter than all four of the distal Co−N bonds to the pyrazine nitrogen atoms (av $Co-Npy_{central}$ = 1.900 Å vs av $Co-Npz_{distal}$ = 2.072 Å).

For comparison, for the parent terpyridine complex $[Co^{II}(\textbf{L1})_2](BF_4)_2$ in the HS state the average $Co-Npy_{central}$ versus average $Co-Npy_{distal}$ is 2.038 versus 2.154 Å whereas for the LS state it is 1.909 versus 2.092 Å (Table 1).[52] The complex of the all-pyridine analogue of **py-pzpypz**, $[Co^{II}(\textbf{L5})_2](ClO_4)_2$, also appears to be *low spin* at 100 K on the basis of the structural data (Table 1),[11] although no magnetic data or comment on the spin state was present in that paper, although there is a Jahn−Teller compression rather than the elongation which is usually observed for terpyridine-like complexes (Table 1). One other notable exception is seen for the reverse spin crossover Co^{II} complex of $\textbf{C}_{14}$**-terpy** (where $\textbf{C}_{14}$**-terpy** is 4′-tetradecyloxy-2,2′:6′,2″-terpyridine) (Table 1).[53] Consistent

Table 1. Comparison of Co−N Bond Lengths in Selected Terpyridine-like Complexes of the Form $[Co(L)_2](BF_4)_2$

L	HS/LS at T (K)	$Co-N_{central}$ (Å)	$Co-N_{distal}$ (Å)
L1[52]	LS at 100	1.906(3), 1.912(2)	2.084(2), 2.088(2), 2.088(2), 2.107(2)
L1[52]	∼HS[a] at 375	2.045(4), 2.030(4)	2.160(3), 2.151(3), 2.149(3), 2.156(3)
L2[33]	LS at 150	1.932(4)	2.099(3)
$\textbf{C}_{14}$**-terpy**[53]	LS at 10	1.910(3), 1.977(4)	2.137(4), 2.114(4), 1.976(4), 1.977(4)
$\textbf{C}_{14}$**-terpy**[53]	HS at 190	2.034(4), 2.020(4)	2.143(4), 2.167(4), 2.123(4), 2.151(4)
L5[11]	LS[b] at 100	1.893(2), 1.901(2)	2.064(2), 2.065(2), 2.083(2), 2.083(2)
py-pzpypz (this work)	LS[c] at 100	1.877(3), 1.923(3)	1.998(3), 2.006(3), 2.149(3), 2.159(2)
py-pzpypz (this work)	LS:HS[c] (70:30) at 265	1.868(2), 1.932(2)	1.977(2), 1.977(2), 2.162(2), 2.169(2)

[a]About 90% HS at 375 K. [b]Magnetic data not reported but distances consistent with LS. [c]Data provided here is for polymorph **1**.

DOI: 10.1021/acs.inorgchem.5b00428
Inorg. Chem. 2015, 54, 5398−5409

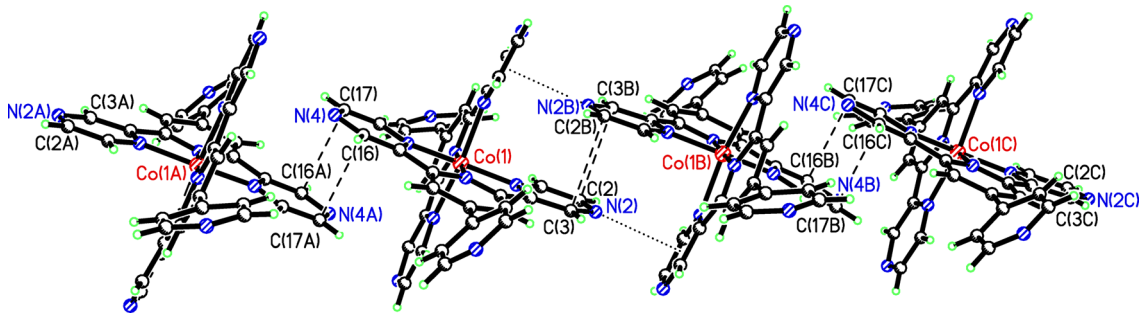

Figure 3. $\pi-\pi$ stacking (dashed lines) and $N_{Pz}-\pi_{Pz}$ (dotted lines) interactions in $[Co(\textbf{py-pzpypz})_2](BF_4)_2\cdot MeCN\cdot CHCl_3$ (polymorph **1**) with anions and solvent molecules omitted for clarity.

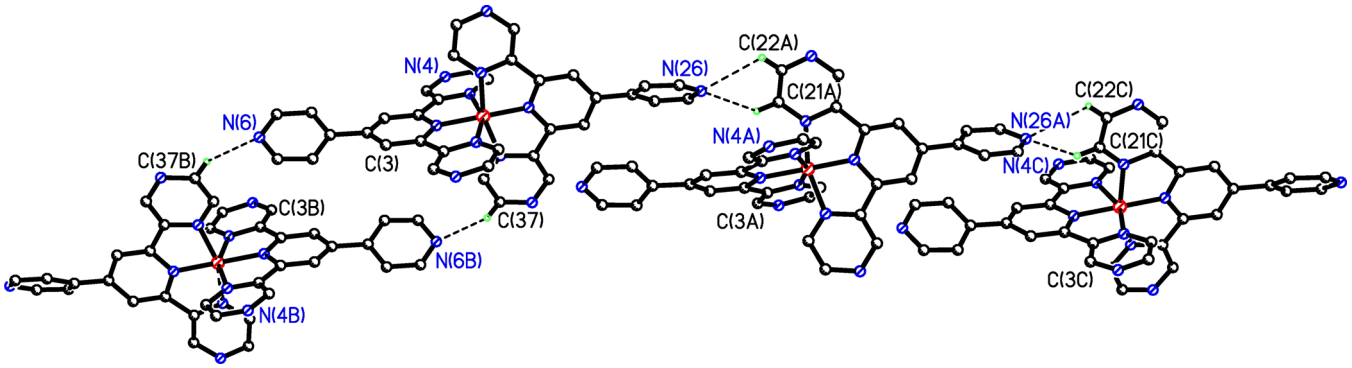

Figure 4. Nonclassical C−H···N hydrogen bonding in solvent-free $[Co^{II}(\textbf{py-pzpypz})_2](BF_4)_2$ (polymorph **2**). Anions and H atoms (except where involved) have been omitted for clarity.

with these specific examples, a search of the CSD (version 5.36, Nov 2014),[54,55] for cobalt(II) bis-terpyridine based complexes, gave 78 hits (LS and HS) with overall averages of $Co^{II}-N_{central}$ = 1.955 Å versus av $Co^{II}-N_{distal}$ = 2.108 Å.

The two polymorphs show significantly different packing interactions (Figures 3 and 4). In the solvated polymorph, polymorph **1** ($P\bar{1}$), offset $\pi-\pi$-stacking interactions between the pyrazine rings (N2 ring with N2′ ring; N4 ring with N4′ ring) result in 1D chains of the complexes (Figure 3 and Table 3). Additionally there appears to be a favorable interaction between the lone pair on one of the "spare" pyrazine nitrogen atoms on one complex (N2) and the π-deficient pyrazine ring of an adjacent complex (Figure 3). This neutral e-rich atom to e-deficient aromatic ring interaction is akin to the acetonitrile lone-pair to π-deficient triazine ring interactions first noted by Gamez, Reedijk, and co-workers,[56] and more recently expanded upon by a CSD survey of the interactions of various neutral e-rich species, including R≡N and R═N—R′, with a range of aromatic rings.[57] The pyrazine N lone-pair to pyrazine centroid distances (Table 3) are consistent with moderate lone-pair to π interactions. The chloroform molecule interacts weakly with one of the tetrafluoroborate anions [Cl_3C—H···F = 3.053(3) Å, 156.8(1)°]. Surprisingly, no significant interactions are observed for the 4-pyridyl nitrogen atoms in polymorph **1** (Supporting Information Figure S8).

The crystal of $[Co^{II}(\textbf{py-pzpypz})_2](BF_4)_2\cdot MeCN\cdot CHCl_3$ (polymorph **1**) was also warmed up and collected at 265 K. At 265 K only a very small increase in cell volume was observed along with very slight increases in all three cell axes (Supporting Information Table S1). A slight decrease in the two long bonds (Table 2) was also observed, consistent with a very small decrease in Jahn−Teller distortion which would be expected for high spin Co(II). It is important to note that at this temperature the magnetic data suggests the sample is only approximately 30% HS, so it is unsurprising that the differences from the 100 K data set are slight.

The π-stacking interactions are weakened in the solvent-free polymorph **2** ($P2_1/n$) such that the closest contact is now N4···C3A (3.247(5) Å, Supporting Information Figure S8). In this polymorph a bifurcated nonclassical C−H···N hydrogen bond is observed between one of the 4-pyridyl nitrogen atoms and two pyrazine C−H protons on an adjacent complex (Figure 4; C(21)−H···N(26) = 3.153(5) Å, 133.0(2)°; C(22)−H···N(26) = 3.335(5), 116.7(3)°]. The other 4-pyridyl nitrogen is involved in a single nonclassical hydrogen bond [C(37)−H···N(6) = 3.149(5) Å, 144.3(3)°]. Together these nonclassical H-bonds result in a 1D chain of complexes (Figure 4). The Co···Co separation along the chain in polymorph **2** is 8.920 Å whereas it was 8.717 Å in polymorph **1**. Interestingly, no pyrazine lone-pair···π interactions are observed in polymorph **2** (Supporting Information Figure S8).

The nickel(II) complex $[Ni(\textbf{py-pzpypz})_2](BF_4)_2\cdot MeCN\cdot CHCl_3$ is isomorphous with the solvated cobalt(II) complex (i.e., polymorph **1**). Hence both the $\pi-\pi$-stacking interactions and the spare pyrazine nitrogen lone pair to the π-electron poor pyrazine ring on an adjacent complex are observed here too (Supporting Information Figure S9, Table 3). Again, the chloroform molecule hydrogen bonds to one of the tetrafluoroborate anions [Cl_3C−H···F = 3.063(3) Å, 153.1(1)°].

While the manganese(II) analogue crystallizes solvent-free (in $P\bar{1}$) and features the most distorted octahedral geometry of all of these complexes (Σ = 160°, Table 2), it too exhibits pyrazine $\pi-\pi$-stacking and pyrazine lone-pair−π(pyrazine) interactions (Supporting Information Figure S10, Table 3). However, the zinc(II) analogue, $[Zn(\textbf{py-pzpypz})_2](BF_4)_2\cdot$

DOI: 10.1021/acs.inorgchem.5b00428
Inorg. Chem. 2015, 54, 5398−5409

Table 2. Selected Structural Data (Distances in Å; Angles in deg) for the $[M^{II}(py\text{-}pzpypz)_2]$ Complexes, $[Mn(py\text{-}pzpypz)_2](ClO_4)_2\cdot 2MeCN$, $[Co(py\text{-}pzpypz)_2](BF_4)_2$ (polymorph 2), $[Co(py\text{-}pzpypz)_2](BF_4)_2\cdot MeCN\cdot CHCl_3$ (polymorph 1), $[Fe(py\text{-}pzpypz)_2](BF_4)_2\cdot$(solvents), $[Ni(py\text{-}pzpypz)_2](BF_4)_2\cdot MeCN\cdot CHCl_3$ and $[Zn(py\text{-}pzpypz)_2](BF_4)_2\cdot 2MeCN$

M^{II}	Mn	Co[c]	Co[d]	Co[d]
T (K)	100	100	100	265
M−Npz	2.272(4)	2.139(4)	2.169(2)	2.159(2)
	2.204(5)	2.153(4)	2.162(2)	2.149(3)
	2.252(4)	1.993(3)	1.977(2)	2.006((3)
	2.262(3)	1.999(4)	1.977(2)	1.998(3)
M−Npy	2.121(4)	1.870(3)	1.931(2)	1.923(3)
	2.186(4)	1.927(3)	1.867(2)	1.877(3)
Npz−M−Npy[a]	72.7(1)	79.1(1)	78.59(7)	79.0(1)
	72.6(1)	78.6(1)	79.10(7)	79.3(1)
	73.1(2)	80.9(1)	81.35(7)	80.8(1)
	72.2(1)	81.3(1)	81.60(7)	81.1(1)
Npz−M−Npz[a]	145.0(1)	157.6(1)	157.58(7)	158.2(1)
	145.2(2)	162.1(1)	162.72(7)	161.8(1)
Npy−M−Npy	171.5(2)	177.9(1)	177.02(9)	177.1(1)
O_h distortion	Σ = 160.1	Σ = 94.9	Σ = 85.5	Σ = 86.6
∠pyr−pyr[b]	53.75	25.54	55.63	54.29
	55.45	42.56	53.77	54.75

M^{II}	Fe	Ni	Zn
T (K)	100	100	100
M−Npz	1.963(5)	2.124(2)	2.179(3)
	1.958(5)	2.120(2)	2.185(3)
	1.972(4)	2.105(2)	2.215(3)
	1.963(5)	2.087(2)	2.231(4)
M−Npy	1.880(5)	1.991(2)	2.078(3)
	1.879(4)	1.986(2)	2.079(3)
Npz−M−Npy[a]	81.1(2)	78.33(7)	74.8(1)
	80.9(2)	78.32(7)	75.2(1)
	81.0(2)	78.27(7)	75.5(1)
	81.2(2)	78.23(7)	76.0(1)
Npz−M−Npz[a]	162.1(2)	156.51(7)	150.2(1)
	162.2(2)	156.51(7)	150.7(1)
Npy−M−Npy	178.2	177.50(7)	175.5(1)
O_h distortion	Σ = 79.2	Σ = 103.3	Σ = 147.0
∠pyr−pyr[b]	47.79	54.46	51.25
	55.81	55.86	51.48

[a]Within a ligand strand. [b]Angle between the mean planes of the pyridine rings within a ligand strand. [c]Polymorph **2**. [d]Polymorph **1**.

2MeCN (Figures 5 and 6), shows a different packing arrangement from the "1D chain of complexes" seen for all

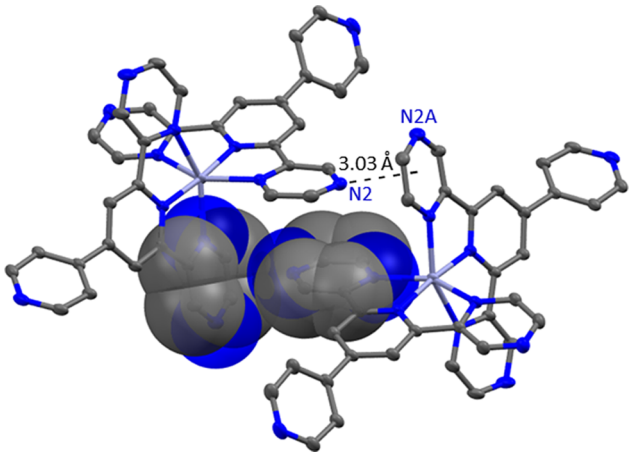

Figure 5. Space filling model of two adjacent molecules of $[Zn(py\text{-}pzpypz)_2](BF_4)_2\cdot 2MeCN$ highlighting the strong pair of intermolecular $N_{Pz}-\pi$ interactions between N(2) and the N(24A) ring on the adjacent complex and, by symmetry, between N(24) and the N(2A) ring.

of the other structures in the $P\bar{1}$ space group [i.e., for Co(II) polymorph **1**, Mn(II) and Ni(II) (Figure 3 and Supporting Information Figures S9 and S10)]. Specifically, in the case of Zn(II) the pyrazine N(2) lone-pair···π(pyrazine) interaction is remarkably strong and results in dimeric pairs of interacting molecules (Figures 5 and 6, Table 3). This results in the N4 and N4′ pyrazine rings being too far apart to interact strongly (centroid···centroid 3.474 Å, but the closest contact Y···Z is significantly longer than the other examples, 3.309 Å, Table 3).

One of the MeCN molecules and both tetrafluoroborate anions are involved in nonclassical C−H···A hydrogen bonds to the main residue (Supporting Information Figure S11).

Single crystals of the iron(II) analogue, $[Fe(py\text{-}pzpypz)_2](BF_4)_2\cdot$solvents, were also grown from vapor diffusion of Et_2O into an MeCN solution, of $[Fe(py\text{-}pzpypz)_2](BF_4)_2\cdot 2H_2O$. These crystals diffracted only weakly, and hence, the quality of data obtained was relatively poor. As a result the crystal packing is not discussed in detail here, but it is isostructural with $[Zn(py\text{-}pzpypz)_2](BF_4)_2\cdot 2MeCN$, and hence shows the same packing, albeit without the strong $N_{Pz}-\pi$ interactions.

Exposure of diethyl ether vapor to a solution of crude $\{[Cu(py\text{-}pzpypz)(solvent)_2](BF_4)_2\}_n$ in DMF resulted in green block shaped crystals of the 1D chain $\{[Cu(py\text{-}pzpypz)(DMF)_2](BF_4)_2(DMF)\}_n$ (Figure 7), with one-half of the $[Cu(py\text{-}pzpypz)(DMF)_2](BF_4)_2(DMF)$ complex in the asymmetric unit, and the other half being generated by a center of inversion.

Table 3. Summary of the $N_{Pz}-\pi$ and $\pi-\pi$ Interactions in the $[M^{II}(py\text{-}pzpypz)_2]X_2$ Complexes[a]

$[M^{II}(py\text{-}pzpypz)_2]X_2$	$[Mn^{II}(py\text{-}pzpypz)](ClO_4)_2$	$[Co^{II}(py\text{-}pzpypz)_2](BF_4)_2$[c]	$[Ni^{II}(py\text{-}pzpypz)_2](BF_4)_2$	$[Zn^{II}(py\text{-}pzpypz)_2](BF_4)_2$
N(2)···centroid(Pz) (Å)	3.185	3.183	3.144	3.030
N(2)···Y, N(2)···Z[b] (Å)	3.089(7), 3.124(7)	3.164(2), 3.169(3)	3.146(3), 3.157(3)	3.088(5), 3.099(3)
$\angle N_{Pz}\cdots Pz$ (deg)	80.58°	81.58°	82.44°	82.62°
centroid···centroid (N4 ring) (Å)	3.412	3.457	3.401	3.474
Y···Z (N4 ring)[b] (Å)	3.04(2)	3.090(3)	3.082(3)	3.309(5)
centroid···centroid (N2 ring) (Å)	3.514	3.581	3.531	3.381
Y···Z (N2 ring)[b] (Å)	3.326(6)	3.288(3)	3.302(3)	3.130(5)

[a]Angles between mean planes of the $\pi-\pi$-stacked rings are 0° by symmetry.[58] [b]Y and Z = closest atom···atom contacts between pyrazine rings. Note the sum of the van de Waals radii (vdW); vdW(C) + vdW(N) = 3.25 Å, vdW(N) + vdW(N) = 3.10 Å. [c]Polymorph **1**.

DOI: 10.1021/acs.inorgchem.5b00428
Inorg. Chem. 2015, 54, 5398−5409

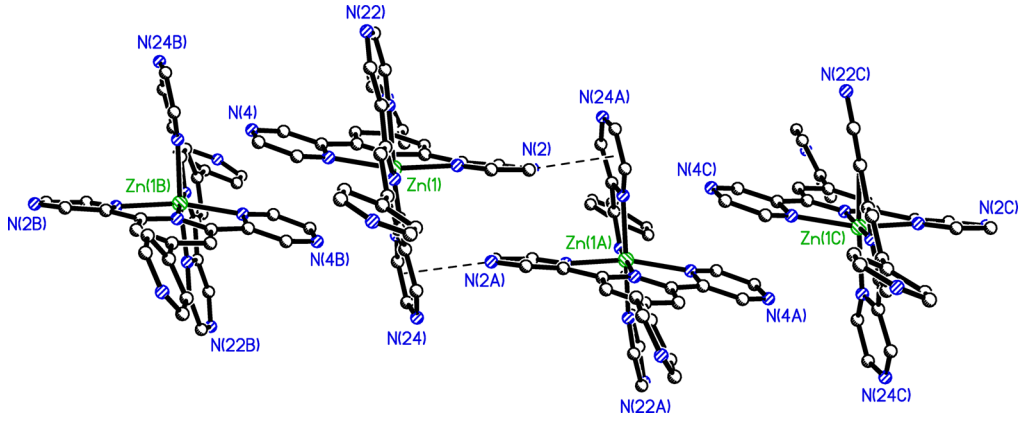

Figure 6. Crystal packing interactions in $[Zn^{II}(\textbf{py-pzpypz})_2](BF_4)_2{\cdot}2MeCN$ with anions, solvent molecules, and H atoms omitted for clarity.

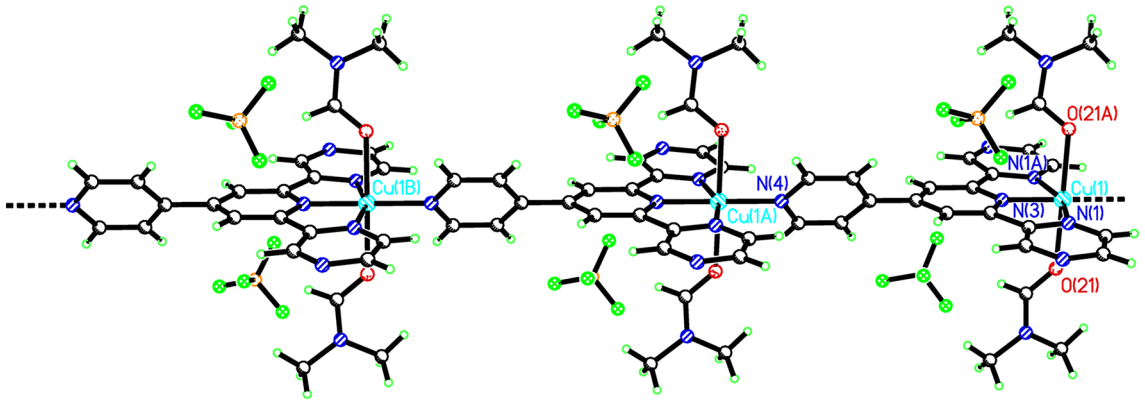

Figure 7. Perspective view of the 1D chain polymer $\{[Cu^{II}(\textbf{py-pzpypz})(DMF)_2](BF_4)_2(DMF)\}_n$.

The copper(II) center adopts a N_4O_2 octahedral coordination environment binding to one tridentate pocket and the 4-pyridyl nitrogen of an adjacent complex, as well as two DMF molecules axially. As is normal for Cu(II), the two axial bonds are significantly longer, Co−O_{21} 2.321 Å, than the bonds in the square plane (Cu−N = 1.940−2.078, Table 2). The bridging by the 4-pyridyl group results in a 1D chain of complexes and well-separated copper centers (Cu···Cu 10.897 Å). No significant π-stacking interactions are observed either within or between individual 1D chains. There are weak bifurcated nonclassical C−H···F hydrogen bonds between one C−H proton on each of the pyrazine and central pyridine rings and the non-coordinating anion [C(3)−H···F(32) = 3.434(3) Å, 170.1°; C(6)−H···F(32) = 3.419(3) Å, 161.6°], as well as weak interchain C−H···N interactions between one C−H proton on the 4-pyridyl group and the "spare" pyrazine nitrogen of an adjacent chain [C(10)−H···N(2) = 3.437(3) Å, 154.4°].

Single crystals of $[Cu(\textbf{py-pzpypz})Cl_2]{\cdot}MeCN$ were picked out from the inhomogeneous mixture obtained from heating $[Cu(H_2O)_4(NO_3)_2]$ and **py-pzpypz** in MeCN to 140 °C in a Teflon lined stainless steel pressure reaction vessel. Presumably there was a trace of chloride present in the reaction vessel. As noted above, a pure sample of this material was subsequently prepared deliberately (Experimental Section).

In this case the complex is mononuclear, not polymeric, but an array of intermolecular interactions produces chains of it (Figure 8, Supporting Information Figure S12). The copper(II) center adopts a square pyramidal coordination sphere with one chloride anion almost in the plane of the terdentate **py-pzpypz** ligand, and the other perpendicular to the square plane (hence

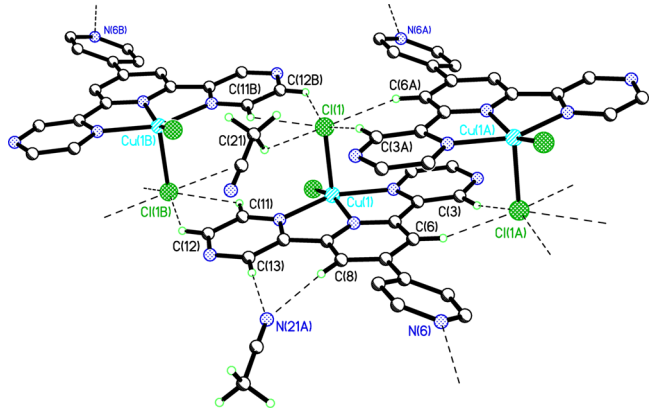

Figure 8. Nonclassical C−H hydrogen bonding in the crystal lattice of $[Cu(\textbf{py-pzpypz})(Cl)_2]{\cdot}MeCN$. H atoms (except where involved) have been omitted for clarity.

axial). As expected, the axial chloride bond is significantly weaker than that of the chloride in the square plane [Cu−Cl(1) = 2.421(1) Å; Cu−Cl(2) = 2.225(1) Å], and the Cu−N bonds in the square plane (1.962−2.060 Å, Table 2).

Interestingly, the intermolecular interactions in the crystal lattice of this compound are almost entirely composed of weak C−H hydrogen bonds between adjacent complexes, generating supramolecular chains (Figure 8, Supporting Information Figure S12). The axial chloride interacts with three aromatic ring C−H protons on two adjacent molecules [C(11)−H···Cl(1) = 3.468(4) Å, 126.3°; C(12)−H···Cl(1) = 3.487(4) Å, 126.8°; C(6′)−H···Cl(1) = 3.504(3) Å, 160.2°] and one

DOI: 10.1021/acs.inorgchem.5b00428
Inorg. Chem. 2015, 54, 5398−5409

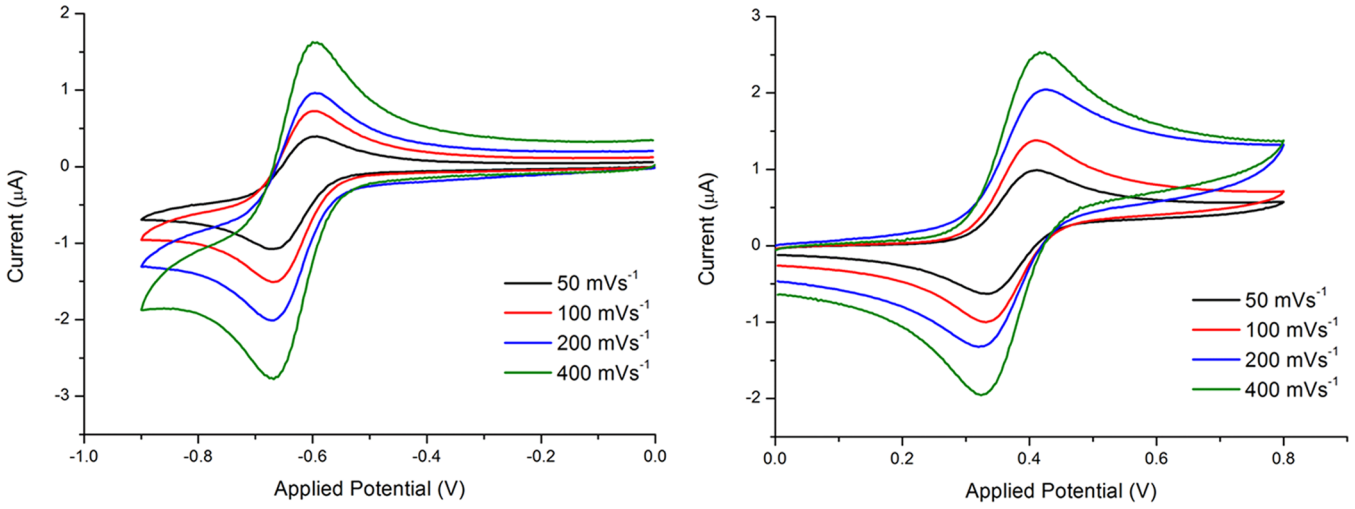

Figure 9. Scan rate studies of the $Co^{I/II}$ (left) and $Co^{II/III}$ (right) redox couples in a 0.45 mmol L^{-1} solution of $[Co^{II}(\mathbf{py\text{-}pzpypz})_2]^{2+}$ in MeCN. Reference is 0.01 M $AgNO_3$/Ag.

acetonitrile solvent molecule [C(21)−H···Cl = 3.461(3) Å, 129.3°]. The acetonitrile molecule also acts as a hydrogen bond acceptor [C(8)−H···N(21) = 3.373(4) Å, 170.0°; C(13)−H···N(21) = 3.425(5) Å, 173.6°]. Also, there is one weak $\pi-\pi$-stacking interaction observed between 4-pyridyl groups on adjacent molecules [centroid−centroid =3.550 Å; shortest contact C(16)−C(14A) = 3.350 Å, Supporting Information Figure S12].

Electrochemistry. It is helpful to note at the outset that none of the processes described below are observed in the analogous Zn^{II} complex (Supporting Information Figure S28) indicating that they are metal-centered (not ligand) oxidations and reductions.

The complex $[Co^{II}(\mathbf{py\text{-}pzpypz})_2](BF_4)_2$ shows two reversible metal based processes (Figure 9). The $Co^{II/III}$ couple is observed at E_m = +0.37 V and the $Co^{I/II}$ process at −0.63 V (Table 4). Interestingly, these two reversible redox processes

Table 4. E_m (V) and [ΔE] (mV) Values in Acetonitrile for the $[M^{II}(\mathbf{py\text{-}pzpypz})_2]^{2+}$ Complexes Reported in This Work, and a Comparison to the E_m (V) Values Reported for the Analogous Complexes of L5[a]

M^{II}	$M^{II/III}$ E_m (V) [ΔE (mV)]	$M^{II/III}$ E_m (V) (for **L5**)[11,59]	$M^{I/II}$ E_m (V) [ΔE (mV)]
Fe	+1.26 [72]	+0.80	
Co	+0.37 [100]	−0.14[b]	−0.63 [76]

[a]All of the tabulated values are referenced to 0.01 M $Ag^+/AgNO_3$. [b]Observed at 0.164 vs SSCE in DMSO and hence 0.302 V was subtracted for comparison to the present data.[60]

are at potentials on either side of, and relatively close to, 0 V. The ΔE values and bulk electrolysis results are consistent with both of these processes being one electron transfers (Supporting Information Figure S16). The latter studies resulted in clear color changes: from orange to peach on oxidation to Co^{III} and to pale yellow on reduction to Co^{I} (Figure 10). Both of these processes are robust reversible redox events, as cyclic voltammograms show them to be unchanged after bulk electrolysis at +0.7 V, forming the Co^{III} species (Supporting Information Figure S17, 0.77 electron equivalents), and after two one electron reductions, first at +0.25 V (Supporting Information Figure S19, 0.68 electron equivalents)

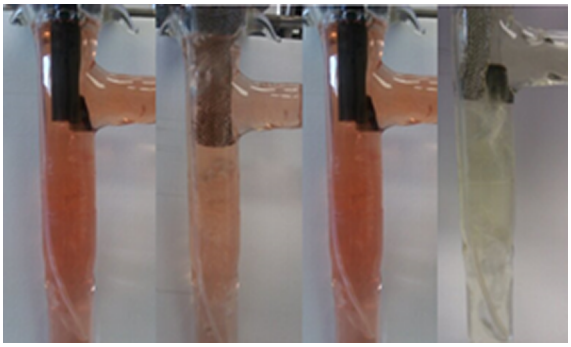

Figure 10. Color changes observed for the bulk electrolysis of $[Co(\mathbf{py\text{-}pzpypz})_2](BF_4)_2$. From left to right: $[Co(\mathbf{py\text{-}pzpypz})_2]^{2+}$, $[Co(\mathbf{py\text{-}pzpypz})_2]^{3+}$ (after bulk electrolysis at 0.70 V), $[Co(\mathbf{py\text{-}pzpypz})_2]^{2+}$ (after bulk electrolysis at 0.25 V), and $[Co(\mathbf{py\text{-}pzpypz})_2]^{+}$ (after bulk electrolysis at −0.90 V).

and then at −0.9 V (Supporting Information Figure S21, 0.79 electron equivalents).

A quasireversible one electron oxidation is observed for $[Fe^{II}(\mathbf{py\text{-}pzpypz})_2](BF_4)_2$ at E_m = +1.26 V. The bulk electrolysis of this solution at +1.65 V resulted in a significant color change from violet Fe^{II} to yellow Fe^{III} (Supporting Information Figure S24) and the transfer of 1.02 electron equivalents.

Due to the stronger π-acceptor nature of pyrazine, the substitution of pyrazine for pyridine is expected to stabilize the lower oxidation states and hence move the redox potentials to higher values. Consistent with this, all of the observed processes for these complexes of the new pyrazine ligand **py-pzpypz** are shifted to considerably more positive potentials than those observed for the previously reported complexes of the analogous all-pyridine ligand, $[M^{II}(\mathbf{L5})_2]^{2+}$ where M = Co[11] and Fe[59] (Table 4).

Magnetic Properties. Several examples of spin crossover have been reported in Co^{II} complexes of terpyridine-type ligands[14,21,23−25] whereas the analogous Fe^{II} complexes are generally low spin.[26] While pyrazine is a poorer σ-donor than pyridine, it is also a stronger π-acceptor[34] so it would generally be expected to better stabilize the low spin state in 3d complexes. However, while Halcrow and co-workers found that

DOI: 10.1021/acs.inorgchem.5b00428
Inorg. Chem. 2015, 54, 5398−5409

replacement of the distal pyridine groups in terpyridine by the stronger π-acceptor pyrazine (**L2**) resulted in low spin complexes of Co^{II}, replacement of the central pyridine by pyrazine resulted in high spin complexes (**L3**) (Table 4).[33] It is intriguing that the complex with central pyrazine donors, $[Co(\mathbf{L3})_2](BF_4)_2$, has by far the lowest $T_{1/2}$ (<50 K) of this family of ligands (Table 5), even far lower than the all pyridine terpyridine complex (**L1**, $T_{1/2}$ = 270 K).

Table 5. Comparison of Spin States and/or $T_{1/2}$ Values for Selected $[Co(LX)_2](BF_4)_2$ (All Solvent-Free) Complexes with the Present $[Co^{II}(\mathbf{py\text{-}pzpypz})_2](BF_4)_2{\cdot}2.5(H_2O)$ and Polymorph 2 (Solvent-Free) Samples (Both with $T_{1/2}$ ~298 K), as a Function of Pyrazine vs Pyridine Rings Present in the Terdentate Ligands

ligand	central	distal	4-R	$T_{1/2}$/K
L3[33]	Pz	Py		<50
L1[52]	Py	Py		270
py-pzpypz	Py	Pz	4-Py	~298
L2[33]	Py	Pz		LS[a]
L4[33]	Pz	Pz		LS[a]

[a]A small amount HS character noted at 298 K.

The effect on cobalt(II) of replacement of the *distal* pyridines by pyrazines in terpyridyl-like ligands is further probed here, usig the new **py-pzpypz** ligand. A potential bonus of the new ligand design is that the "spare" nitrogen donors, in both the pair of pyrazine rings and the 4-pyridyl substituent off the back of the central pyridine ring in **py-pzpypz**, provide additional hydrogen-bond acceptors which may increase intermolecular interactions and lead to thermal hysteresis, which is only rarely observed for Co^{II}.[14,25,39]

The molar magnetic susceptibility was therefore measured on a sample of air-dried crystals of polymorph **1** which analyzed as $[Co^{II}(\mathbf{py\text{-}pzpypz})_2](BF_4)_2{\cdot}2.5(H_2O)$, a sample of solvent-free polymorph **2**, and on $[Fe^{II}(\mathbf{py\text{-}pzpypz})_2](BF_4)_2{\cdot}2H_2O$. The complex $[Fe^{II}(\mathbf{py\text{-}pzpypz})_2](BF_4)_2{\cdot}2H_2O$ was unsurprisingly LS at room temperature.

In contrast, both samples of the cobalt(II) complex are SCO active, and give similar χ_mT versus T plots (Figure 11 and Supporting Information Figure S13), despite having substantial differences in crystal packing and solvent content (both factors have been shown to be very important in other cases[61−65]). Hence, only the air-dried sample of polymorph **1** is described in detail here. The sample of $[Co^{II}(\mathbf{py\text{-}pzpypz})_2](BF_4)_2{\cdot}2.5(H_2O)$ obtained on air drying the crystals of polymorph **1** undergoes a gradual spin crossover (Figure 11), with χ_mT decreasing from 1.44 $cm^3\ mol^{-1}\ K$ at 375 K (μ_{eff} = 3.40 μ_B), consistent with approximately 75% HS, to 0.38 $cm^3\ mol^{-1}\ K$ at 4 K (μ_{eff} = 1.74 μ_B), consistent with being fully LS. At 298 K χ_mT is 1.06 $cm^3\ mol^{-1}\ K$, ~50% HS, so the $T_{1/2}$ is approximately room temperature for this complex (as the fully HS state could not be achieved, a χ_mT value of 2.6 $cm^3\ mol^{-1}\ K$ was used to estimate the $T_{1/2}$). The gradual nature of this SCO is consistent with that observed in many other Co(II) terpyridine derivatives.[14,21,33]

The presence of the *distal* pyrazine nitrogen donors in **py-pzpypz** has stabilized the LS state only slightly, as $T_{1/2}$ only increased by ~30 K when compared to the analogous all pyridine donor terpyridine complex, $[Co(\mathbf{L1})_2](BF_4)_2$ ($T_{1/2}$ = 270 K).[52] Interestingly, the other analogues that feature *distal* pyrazine donors, $[Co^{II}(\mathbf{L2})_2](BF_4)_2$ and $[Co^{II}(\mathbf{L4})](BF_4)_2$,

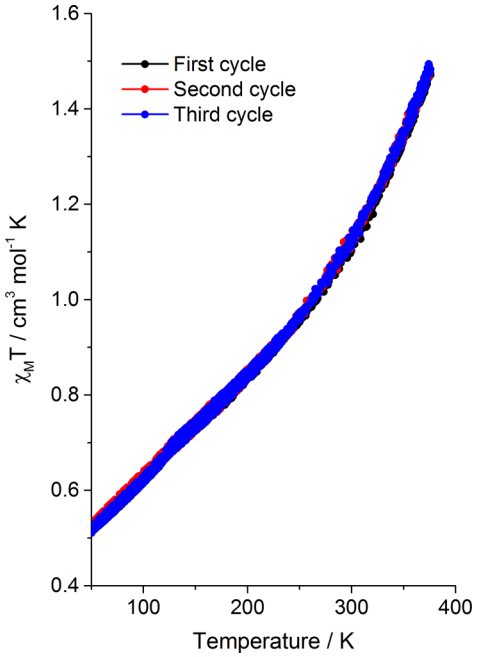

Figure 11. Molar susceptibility product χ_mT as a function of temperature, over three consecutive cycles of 50 to 375 to 50 K, for a crystalline sample of $[Co^{II}(\mathbf{py\text{-}pzpypz})_2](BF_4)_2{\cdot}2.5(H_2O)$ obtained on air drying the crystals of polymorph **1**.

remain almost fully LS up to 300 K (Table 5),[33] so **py-pzpypz** is not as effective at stabilizing the LS state as those ligands are. This may well be due in part to differences in packing interactions due to the presence of the 4-pyridyl moiety "out the back" of **py-pzpypz**.

Interestingly, the fine balance of the ligand field provided to cobalt(II) by two **py-pzpypz** ligands has led to the SCO event being centered close to ambient temperature. However, despite the intermolecular interactions achieved by through the noncoordinating nitrogen atoms (Figures 3 and 4), the SCO shows the gradual nature that is characteristic of many Co^{II} terpyridine-type complexes.

CONCLUSION

The synthesis and structural characterization of a new ligand 4-(4-pyridyl)-2,5-dipyrazyl-pyridine (**py-pzpypz**) and seven first row transition metal complexes of it are reported, along with magnetic and electrochemical characterization of the complexes.

In all of the complexes investigated, except for copper(II), a 2:1 L:M reaction stoichiometry leads to an $[ML_2]^{2+}$ product, resulting in six "spare" N donors pointing out approximately along the axes of an octahedron. This results in a range of interesting crystal packing interactions, most notably lone-pair···π(pyrazine) interactions. These "spare" N donors also endow the complexes with the potential to be used as secondary building units (SBUs[66]) for subsequent assembly into supramolecular architectures as we have recently demonstrated with imide complexes.[40,43]

In the case of copper(II), despite a 2:1 L:M reaction, the products obtained were 1:1. With tetrafluoroborate counterions the product is a 1D chain polymer, featuring bridging of the N_4O_2 octahedral copper(II) centers by the 4-pyridyl donors "out the back", whereas with chloride counterions discrete

DOI: 10.1021/acs.inorgchem.5b00428
Inorg. Chem. 2015, 54, 5398−5409

Table 6. Crystal Structure Determination Details for the 10 Structures Reported Herein

	[Mn(**py-pzpypz**)$_2$](ClO$_4$)$_2$	[Fe(**py-pzpypz**)$_2$](BF$_4$)$_2$	[Co(**py-pzpypz**)$_2$](BF$_4$)$_2$MeCN·CHCl$_3$ (Polymorph **1**)	[Co(**py-pzpypz**)$_2$](BF$_4$)$_2$MeCN·CHCl$_3$ (Polymorph **1**)	[Co(**py-pzpypz**)$_2$](BF$_4$)$_2$
formula	$C_{40}H_{30}Cl_2MnN_{14}O_8$	$C_{36}H_{24}FeN_{12}$	$C_{39}H_{28}B_2Cl_3CoF_8N_{13}$	$C_{39}H_{28}B_2Cl_3CoF_8N_{13}$	$C_{36}H_{24}B_2CoF_8N_{12}$
M_r (g mol^{-1})	960.62	680.52	1017.64	1017.64	857.22
cryst syst	triclinic	triclinic	triclinic	triclinic	monoclinic
space group	$P\bar{1}$	$P\bar{1}$	$P\bar{1}$	$P\bar{1}$	$P2_1/n$
T/K	100(2)	100(2)	100(2)	265(2)	100(2)
a/Å	12.9056(5)	12.4714(12)	12.6348(4)	12.7499(5)	16.9153(5)
b/Å	13.0957(5)	12.6899(5)	12.7543(4)	12.8625(4)	8.9203(2)
c/Å	13.4141(4)	15.2546(11)	13.2880(4)	13.4273(5)	23.4566(6)
α/deg	82.7200(3)	78.116(5)	83.011(3)	83.253(3)	90
β/deg	83.386(3)	68.027(8)	87.272(2)	87.858(3)	101.141(3)
γ/deg	74.063(3)	75.290(6)	77.918(3)	77.550(3)	90
V/Å^3	2154.61	2148.8(3)	2077.80(11)	2135.18(13)	3472.65(16)
Z	2	2	2	2	4
ρ_{calcd} [g cm^{-3}]	1.481	1.052	1.627	1.583	1.640
μ [mm^{-1}]	4.228	3.102	5.772	5.616	4.699
GOF (F^2)	1.035	1.051	1.026	1.035	1.045
R1 [$I > 2\sigma(I)$]	0.0812	0.1001	0.0415	0.0668	0.0704
wR2 [$I > 2\sigma(I)$]	0.2278	0.2836	0.1109	0.1802	0.1826
R1 [all data]	0.0919	0.1238	0.0439	0.0800	0.0877
wR2 [all data]	0.2418	0.3000	0.1134	0.2001	0.1975

	[Cu(**py-zpypz**)(DMF)$_2$](BF$_4$)$_2$·DMF	[Cu(**py-pzpypz**)$_2$Cl$_2$]·MeCN	[Ni(**py-pzpypz**)$_2$](BF$_4$)$_2$·MeCN·CHCl$_3$	[Zn(**py-pzpypz**)$_2$](BF$_4$)$_2$·2MeCN	**py-pzpypz**·HCl·H$_2$O
formula	$C_{30}H_{40}B_2CuF_8N_{10}O_4$	$C_{20}H_{15}N_7Cl_2Cu$	$C_{39}H_{28}B_2Cl_3F_8N_{13}Ni$	$C_{40}H_{30}B_2F_8N_{14}Zn$	$C_{18}H_{14}Cl_1N_6O_1$
M_r (g mol^{-1})	841.88	487.83	1017.42	945.77	366.81
cryst syst	monoclinic	triclinic	triclinic	triclinic	triclinic
space group	$I2/a$	$P\bar{1}$	$P\bar{1}$	$P\bar{1}$	$P\bar{1}$
T/K	100(2)	100(2)	100(2)	100(2)	100(2)
a/Å	16.3625(1)	7.8448(3)	12.6488(3)	12.5541(5)	5.0852(2)
b/Å	10.8968(1)	11.3531(4)	12.7878(3)	13.0402(6)	8.7458(2)
c/Å	21.5483(2)	12.3304(5)	13.3721(4)	14.6124(9)	19.6004(5)
α/deg	90	67.581(4)	83.081(2)	66.737(5)	91.816(2)
β/deg	108.094(1)	78.421(3)	87.073(2)	81.932(4)	91.053(2)
γ/deg	90	81.235(3)	76.993(2)	72.687(4)	106.868(3)
V/Å^3	3652.04(5)	991.03(7)	2091.46(9)	2097.41(18)	833.44(4)
Z	6	2	2	2	2
ρ_{calcd} [g cm^{-3}]	1.531	1.635	1.498	1.498	1.462
μ [mm^{-1}]	0.690	1.395	1.563	1.563	2.210
GOF (F^2)	1.117	1.063	1.028	1.028	1.067
R1 [$I > 2\sigma(I)$]	0.0477	0.0438	0.0587	0.0587	0.0497
wR2 [$I > 2\sigma(I)$]	0.1428	0.1286	0.1479	0.1479	0.1248
R1 [all data]	0.0489	0.0482	0.0784	0.0784	0.0546
wR2 [all data]	0.1455	0.1345	0.1636	0.1636	0.1271

[CuLCl$_2$] complexes of square pyramidal copper(II) centers are obtained.

The [Fe^{II}(**py-pzpypz**)$_2$](BF$_4$)$_2$ complex is low spin whereas a gradual spin crossover, over the range 50−375 K, is observed for [Co^{II}(**py-pzpypz**)$_2$](BF$_4$)$_2$. A quasireversible Fe$^{II/III}$ process is observed in the iron(II) complex. Two reversible one electron redox processes, attributed to the Co$^{I/II}$ and Co$^{II/III}$, are observed in the cobalt(II) complex. The potentials at which these occur are about 450 mV higher than those observed in the corresponding complexes of the analogous all-pyridine ligand, consistent with the replacement of two pyridine rings by pyrazine rings significantly stabilizing the lower oxidation states.

EXPERIMENTAL SECTION

Except where noted, all chemicals, including pyrazine and pyridine-4-carbaldehyde, were of reagent grade and used as received without further purification. 2-Acetylpyrazine was prepared from pyrazine according to the published procedure.[47] Methanol and acetonitrile were HPLC grade.

X-ray crystal structure determination details (structures refined with SHELXL[67,68]) are provided in Table 6. For full instrument details, for this and other studies, and for the numbering used in the NMR assignments please see the Supporting Information.

Synthesis of 4-(4-Pyridyl)-2,6-di(2-pyrazinyl)pyridine (py-pzpypz). A pale yellow solution of 2-acetylpyrazine (600 mg, 4.91 mmol) and pyridine-4-carbaldehyde (267 mg, 2.49 mmol) in MeOH (8 mL) was prepared by stirring at room temperature (RT) for 5 min.

DOI: 10.1021/acs.inorgchem.5b00428
Inorg. Chem. 2015, 54, 5398−5409

To this solution was added a solution of KOH (2.13 g, 38 mmol) in H_2O (14.4 mL) and saturated aqueous ammonia solution (1.6 mL). The solution turned dark red, and a precipitate began to form almost immediately. The reaction vessel was loosely stoppered and stirred at RT for 24 h. Then H_2O (8 mL) was added and the suspension extracted with $CHCl_3$ (6 × 70 mL), and the combined organic extracts were dried over Na_2SO_4 and filtered to give a clear pale yellow solution. Removal of the solvent at reduced pressure gave the crude product as a pale yellow solid. This was suspended in acetone (20 mL), sonicated for 5 min, filtered, washed with acetone (3 × 10 mL), and dried *in vacuo* to give 4-(4-pyridyl)-2,6-di(2-pyrazinyl)pyridine (**py-pzpypz**) as a white powder (456 mg, 1.46 mmol, 58.6%). Anal. Calcd (%) for $C_{18}H_{12}N_6$ (312.33): C 69.22, H 3.87, N 26.91. Found: C 69.42, H 3.87, N 26.83. ^{1}H NMR (400 MHz, $CDCl_3$): δ (ppm) 9.89 (2H, d, *J*H3−H2 = 1.4 Hz, 2 × H3), 8.80 (2H, *J*H10−H9A = 4.4 Hz, *J*H10−H9B = 1.7 Hz, 2 × H10), 8.77 (2H, s, 2 × H6), 8.70 (4H, m, 2 × H1, 2 × H2), 7.78 (2H, *J*H9−H10A = 4.4 Hz, *J*H9−H10B = 1.7 Hz, 2 × H9). ^{13}C NMR (100 MHz, $CDCl_3$): δ (ppm) 119.7 (C6), 121.5 (C9), 143.6 (C3), 143.6 (C1/C2), 145.1 (C1/C2), 145.3 (C8), 148.1 (C7), 150.3 (C5), 150.8 (C10), 154.9 (C4). HR-ESI-MS (pos) m/z = 335.1044, calcd for $[C_{18}H_{12}N_6Na]^+$ = 335.1016. ATR-IR (ν/cm^{-1}): 3075(w), 1594(m), 1533(w), 1503(w) 1432(w), 1375(m), 1325(w), 1247(w), 1127(w), 1112(m), 1034(m), 1019(s), 856(m), 813(s), 687(m), 813(s), 687(m), 621(s), 579(m), 473(m), 398(s). Colorless block shaped single crystals of **py-pzpypz**·HCl·H_2O, suitable for X-ray crystallography, were grown by vapor diffusion of HCl (from a dilute aqueous HCl solution) into a $CHCl_3$ solution of **py-pzpypz**.

[Fe(py-pzpypz)$_2$](BF$_4$)$_2$·2H$_2$O. A colorless solution of **py-pzpypz** (50.5 mg, 16.2 mmol) in a mixture of MeOH and $CHCl_3$ (1:1, 60 mL) was bubbled with N_2(g) for 10 min. A pale blue solution of $[Fe(H_2O)_6](BF_4)_2$ (26.6 mg, 0.079 mmol) in MeOH (2 mL) was also bubbled with N_2(g) for 5 min before being added to the first solution, resulting in the immediate formation of a dark purple precipitate. A nitrogen balloon was attached, the N_2 flow stopped, and the vessel stirred at RT for 2 h. The dark purple powder was filtered, dried under a flow of N_2(g), and then further dried under vacuum (34.1 mg, 47.7%). Anal. Calcd (%) for [Fe(**py-pzpypz**)$_2$](BF$_4$)$_2$·2H$_2$O ($C_{36}H_{28}N_{12}O_2FeB_2F_8$, 890.15 g mol^{-1}): C 48.58, H 3.17, N 18.88. Found: C 48.96, H 3.11, N 18.59. HR-ESI-MS (pos) m/z = 340.0791, calcd for $[C_{36}H_{24}N_{12}Fe]^{2+}$ = 340.0793. ATR-IR (ν/cm^{-1}): 3618(w), 3078(w), 1599(m), 1485(w), 1428(w), 1405(m), 1356(w), 1295(w), 1195(m), 1055(s, br), 824(s, sh), 647(w), 636(w), 522(w), 499(m), 465(m). ^{1}H NMR (400 MHz, CD_3CN): δ (ppm) 9.71 (4H, d, *J*H3−H2 = 1.1 Hz, 4 × H3), 9.37 (4H, s, 4 × H6), 9.08 (4H, dd, *J*H10−H9A = 4.4 Hz, *J*H10−H9B = 1.7 Hz, 4 × H10), 8.31 (4H, d, *J*H1−H2 = 3.2 Hz, 4 × H1), 8.24 (4H, dd, *J*H9−H10A = 4.4 Hz, *J*H9−H10B = 1.7 Hz, 4 × H9), 7.32 (4H, dd, *J*H2−H1 = 3.2 Hz, *J*H2−H3 = 1.1 Hz, 4 × H2). TGA, Δmass found 4.2%, calcd for 2H_2O 4.1%. Violet, needle shaped, crystals of [Fe(**py-pzpypz**)$_2$](BF$_4$)$_2$·(solvents) suitable for X-ray crystallography were obtained by Et_2O vapor diffusion into an MeCN solution of [Fe(**py-pzpypz**)$_2$](BF$_4$)$_2$·2H_2O.

[Co(py-pzpypz)$_2$](BF$_4$)$_2$·2.5H$_2$O. To a colorless solution of **py-pzpypz** (200 mg, 0.64 mmol) in a mixture of MeOH (75 mL) and $CHCl_3$ (125 mL) was added $[Co(H_2O)_6](BF_4)_2$ (109 mg, 0.32 mmol) in MeOH (25 mL) resulting in the immediate formation of a brick red precipitate. The suspension was stirred at ambient temperature for 2 h and then filtered and washed with $CHCl_3$/MeOH (1:1, 2 × 2 mL). The resulting red solid was air-dried and then further dried under vacuum (241 mg, 0.26 mmol, 81%). Anal. Calcd (%) for [Co(**py-pzpypz**)$_2$](BF$_4$)$_2$·2.5H$_2$O ($C_{36}H_{29}N_{12}O_{2.5}CoB_2F_8$, 902.24 g mol^{-1}): C 47.92, H 3.24, N 18.63. Found: C 47.99, H 2.88, N 18.43. HR-ESI-MS (pos) m/z = 341.5772, calcd for $[C_{36}H_{24}N_{12}Co]^{2+}$ = 341.5784. ATR-IR (ν/cm^{-1}): 3607(w, br), 3086(w), 1620(w), 1599(m), 1473(w), 1403(s), 1190(w), 1035(s, br), 823(s), 482(m), 418(m). TGA, Δmass found 5.2%, calcd for 2.5H_2O 5.0%. Red needle shaped crystals of the solvent-free polymorph **2** suitable for X-ray crystallography were obtained by Et_2O vapor diffusion into an MeCN solution of [Co(**py-pzpypz**)$_2$](BF$_4$)$_2$. Red block shaped crystals of [Co(**py-pzpypz**)$_2$](BF$_4$)$_2$·MeCN·$CHCl_3$ (polymorph **1**) suitable for X-ray crystallography were grown by vapor diffusion of $CHCl_3$ into an MeCN solution of [Co(**py-pzpypz**)$_2$](BF$_4$)$_2$. After air drying the crystals of polymorph **1**, the sample analyzed as [Co(**py-pzpypz**)$_2$](BF$_4$)$_2$·2.5H_2O. Anal. Calcd (%) for $C_{36}H_{29}N_{12}O_{2.5}CoB_2F_8$ (902.24): C 47.97, H 2.88, N 18.63. Found: C 47.80, H 3.14, N 18.33.

[Ni(py-pzpypz)$_2$](BF$_4$)$_2$·2H$_2$O. To a white suspension of **py-pzpypz** (38.8 mg, 0.124 mmol) in 60 mL of MeCN at reflux was added a blue solution of $[Ni(H_2O)_6](BF_4)_2$ (21 mg, 0.064 mmol) in 10 mL of MeCN. After approximately 10 min the yellow suspension cleared to give a golden solution which was refluxed for 22 h. This solution was reduced in volume to 30 mL by rotary evaporation and then subjected to $CHCl_3$ vapor diffusion, resulting in formation of golden-yellow block shaped crystals of [Ni(**py-pzpypz**)$_2$](BF$_4$)$_2$·MeCN·$CHCl_3$ suitable for X-ray crystallography. The crystals were filtered, air-dried, and then further dried under vacuum (43.0 mg, 0.042 mmol, 67%). The solvent molecules are replaced by H_2O on exposure to air. Anal. Calcd for [Ni(**py-pzpypz**)$_2$](BF$_4$)$_2$·2H_2O ($C_{36}H_{28}N_{12}B_2F_8O_2Ni$, 892.99 g mol^{-1}) (%): C 48.42, H 3.16, N 18.82. Found: C 48.58, H 2.97, 18.91. HR-ESI-MS (pos) m/z = 341.0812, calcd for $[C_{36}H_{24}N_{12}Ni]^{2+}$ = 341.0795. ATR-IR (ν/cm^{-1}) = 1619 (w), 1600 (m, sh), 1542 (w), 1476 (w, sh), 1401 (m, br), 1186 (w, br), 1048 (vs, br), 845 (s, sh), 626 (m, sh), 477 (m), 421 (s, sh). TGA, Δmass found 3.6%, calcd for 2H_2O 4.0%

[Mn(py-pzpypz)$_2$](ClO$_4$)$_2$·1.5H$_2$O. ***Caution!*** *While no problems were encountered in the course of this work perchlorate mixtures are potentially explosive and should therefore be handled with appropriate care.*

A white suspension of **py-pzpypz** (60.4 mg, 0.19 mmol) in MeCN (30 mL) at reflux was bubbled with Ar(g) for 5 min before $[Mn(H_2O)_6](ClO_4)_2$ (35.9 mg, 99 μmol) in MeCN (2 mL) was added. Upon addition of the metal salt the suspension immediately cleared to give a yellow solution. Ar(g) bubbling was continued for a further 2 min before an Ar balloon was attached, the Ar flow stopped, and the solution refluxed for 1 h. The solution was allowed to cool to RT and then subjected to vapor diffusion of ^{i}Pr$_2$O, resulting in yellow block shaped crystals of [Mn^{II}(**py-pzpypz**)$_2$](ClO$_4$)$_2$·2MeCN suitable for X-ray crystallography after 2 days. These were filtered and washed with Et_2O/DCM (1:1, 3 × 15 mL), then air-dried to give [Mn(**py-pzpypz**)$_2$](ClO$_4$)$_2$ 1.5H_2O as a yellow powder (the crystals collapse on drying as lattice MeCN is replaced by H_2O (43 mg, 49 μmol, 49.4%). Anal. Calcd for [Mn(**py-pzpypz**)$_2$](ClO$_4$)$_2$·1.5H_2O ($C_{36}H_{27}N_{12}B_2F_8O_{1.5}Mn$, 881.24 g mol^{-1}) (%): C 49.07, H 3.20, N 19.07. Found: C 49.27, H 3.26, N 18.98. HR-ESI-MS (pos) m/z = 339.5807, calcd for $[C_{36}H_{24}N_{12}Mn]^{2+}$ = 339.5808; m/z = 778.1070, calcd for $[C_{36}H_{24}N_{12}MnClO_4]^+$ = 778.1100. ATR-IR (ν/cm^{-1}) = 3078(w, br), 2918(w), 2850(w), 1617(m), 1477(m), 1402(m), 1172(m), 1080(vs), 1032(s, sh), 854(m), 821(m, sh), 619(s, sh), 478(m, sh), 409(s, sh). TGA was not carried out on this material due to the potential explosion risk of perchlorate salts when heated.

[Zn(py-pzpypz)$_2$](BF$_4$)$_2$·1.5H$_2$O. To a colorless solution of **py-pzpypz** (40 mg, 128 μmol) in a mixture of MeOH and $CHCl_3$ (1:1, 50 mL) was added $[Zn(H_2O)_6](BF_4)_2$ (22 mg, 64 μmol) in MeOH (2 mL) resulting in the immediate formation of a white precipitate. The suspension was stirred at RT for 2 h, then filtered, and the solid washed with $CHCl_3$ (2 mL) and MeOH (2 mL). The resulting white solid was air-dried and then further dried under vacuum (31 mg, 35 μmol, 54%). Anal. Calcd (%) for [Zn(**py-pzpypz**)$_2$](BF$_4$)$_2$·1.5H_2O ($C_{37}H_{27}N_{12}O_{1.5}FeB_2F_8$, 890.68 g mol^{-1}): C 48.55, H 3.06, N 18.87. Found: C 48.47, H 2.91, N 18.60. HR-ESI-MS (pos) m/z = 344.0735, calcd for $[C_{36}H_{24}N_{12}Zn]^{2+}$ = 344.0764. ^{1}H NMR (400 MHz, CD_3CN): δ (ppm) 10.0 (4H, d, *J*H3−H2 = 1.4 Hz, 4 × H3), 9.22 (4H, s, 4 × H6), 9.04 (4H, dd, *J*H10−H9A = 4.4 Hz, *J*H10−H9B = 1.7 Hz, 4 × H10), 8.77 (4H, d, *J*H1−H2 = 2.6 Hz, 4 × H1), 8.15 (4H, dd, *J*H9−H10A = 4.4 Hz, *J*H9−H10B = 1.7 Hz, 4 × H9), 7.86 (4H, dd, *J*H2−H1 = 2.6 Hz, *J*H2−H3 = 1.4 Hz, 4 × H2). ^{13}C NMR (100 MHz, CD_3CN): δ (ppm) 154.51, 151.28, 149.34, 148.76, 145.35, 142.84, 142.35, 141.76, 123.26, 122.07. ATR-IR (ν/cm^{-1}) = 3100 (w), 1619 (w), 1600 (m, sh), 1478(w), 1402(m), 1150(w), 1034(vs, br), 823(s, sh), 623(w, sh), 471(m), 415(s, sh). TGA, Δmass found 2.9%, calcd for 1.5H_2O 3.1%. Colorless block shaped crystals of [Zn(**py-**

DOI: 10.1021/acs.inorgchem.5b00428
Inorg. Chem. 2015, 54, 5398−5409

pzpypz)$_2$](BF$_4$)$_2$·2MeCN were grown by vapor diffusion of Et$_2$O into an MeCN solution of the white solid.

{[Cu(py-pzpypz)(H$_2$O)$_2$](BF$_4$)$_2$}$_n$. A green suspension of **py-pzpypz** (50 mg, 0.16 mmol) and copper tetrafluoroborate hydrate (56.5 mg, 0.16 mmol) in DMF (12 mL) was stirred at RT for 75 min. The resulting green solution was subjected to vapor diffusion of Et$_2$O, and green microcrystalline solid was obtained after 1 week. The solid was filtered and then dissolved in DMF (25 mL) and subjected to Et$_2$O vapor diffusion. After 2 weeks the resulting green block shaped crystals of {[Cu(**py-pzpypz**)(DMF)$_2$](BF$_4$)$_2$·DMF}$_n$, suitable for X-ray crystallography, were obtained. These crystals were filtered and washed with DCM (2 × 20 mL) and Et$_2$O (20 mL) and then air-dried. The crystals collapse to a green powder on drying. Further drying *in vacuo* followed by exposure to air resulted in substitution of the two coordinated DMF molecules for H$_2$O (51.0 mg, 0.073 mmol, 46%). Anal. Calcd (%) for {[Cu(**py-pzpypz**)(H$_2$O)$_2$](BF$_4$)$_2$}$_n$ ($C_{18}H_{16}N_6O_2B_2F_8Cu$, 585.52 g mol^{-1}): C 37.10, H 2.49, N 14.71. Found: C 36.92, H 2.75, N 14.35. ATR-IR (ν/cm^{-1}) = 3101(w), 1617(m, sh), 1404(m), 1066(vs), 1040(vs, br), 846(m, sh), 676 (m), 517(m, sh), 494(s, sh), 421(s, sh).

[Cu(py-pzpypz)Cl$_2$]·DCM. A sample tube was loaded with a solution of **py-pzpypz** (30 mg, 0.096 mmol) in DCM/MeOH (4:1, 20 mL). On this was layered a buffer of DCM/MeOH (1:1, 6 mL) and then a layer of CuCl$_2$ (16.4 mg, 0.096 mmol) in MeOH (3 mL). The tube was sealed, and the solutions were allowed to slowly diffuse together, which resulted in green microcrystals after 48 h. These were filtered and washed with MeOH (3 × 5 mL) and DCM (3 × 10 mL), then air-dried (32 mg, 0.072 mmol, 75%). Anal. Calcd (%) for [Cu(**py-pzpypz**)Cl$_2$]·DCM ($C_{19}H_{14}N_6Cl_4Cu$, 446.85 g mol^{-1}): C 42.92, H 2.65, N 15.81. Found: C 42.17, H 2.75, N 15.85. HR-ESI-MS (pos) m/z = 410.0068; calcd for $[Cu(C_{18}H_{12}N_6)Cl]^+$ = 410.0102. ATR-IR (ν/cm^{-1}) = 3019 (m), 1598 (m, sh), 1472 (w, sh), 1457 (m), 1404 (m), 1395(m), 1176(m), 1151(m, sh), 1039(s, sh), 831.31(s), 627(w), 463(s), 410(s). A single crystal sample of [Cu(py-pzpypz)Cl$_2$]·MeCN was obtained serendipitously: To a Teflon-lined stainless steel reaction vessel was added [Cu(H$_2$O)$_4$(NO$_3$)$_2$] (11.6 mg, 45 μmol), **py-pzpypz** (14.0 mg 45 μmol), and MeCN (15 mL). The pressure vessel was sealed and heated at 140 °C for 72 h and then allowed to slowly cool to RT, resulting in an inhomogeneous mixture, including a few green plate shaped single crystals which were suitable for X-ray crystallography.

■ ASSOCIATED CONTENT

Supporting Information

Instrument details, cif files, crystallographic data, additional structure diagrams, additional electrochemical and magnetic figures, and NMR spectra. The Supporting Information is available free of charge on the ACS Publications website at DOI: 10.1021/acs.inorgchem.5b00428.

■ AUTHOR INFORMATION

Corresponding Author

*E-mail: sbrooker@chemistry.otago.ac.nz.

Notes

The authors declare no competing financial interest.

■ ACKNOWLEDGMENTS

We are grateful to the University of Otago for funding this research (including the award of a University of Otago postgraduate scholarship to R.G.M.). We thank the Campbell Microanalytical Laboratory (University of Otago) for performing the microanalyses. We thank Dr. Humphrey L. C. Feltham and Mr. Ross W. Hogue for collecting the magnetic data, the MacDiarmid Institute for funding the magnetometers, and Dr. Jeffrey L. Tallon for facilitating access to them.

■ REFERENCES

(1) Morgan, G. T.; Burstall, F. H. *J. Chem. Soc.* **1932**, 20.
(2) Krohnke, F. *Synthesis* **1976**, 1.
(3) Potts, K. T. *Bull. Soc. Chim. Belg.* **1990**, *99*, 741.
(4) Constable, E. C.; Ward, M. D. *J. Chem. Soc., Dalton Trans.* **1990**, 1405.
(5) Constable, E. C. *Chem. Soc. Rev.* **2007**, *36*, 246.
(6) Sauvage, J.-P.; Collin, J.-P.; Chambron, J.-C.; Guillerez, S.; Coudret, C.; Baltani, V.; Barigelletti, F.; Cola, L. D.; Flamigni, L. *Chem. Rev.* **1994**, *94*, 993.
(7) Limburg, J.; Vrettos, J. S.; Liable-Sands, L. M.; Rheingold, A. L.; Crabtree, R. H.; Brudvig, G. W. *Science* **1999**, *283*, 1524.
(8) *Terpyridine, Oligopyridine and Polypyridine Ligands*; Thummel, R. P., Ed.; Elsevier: Oxford, 2004; Vol. *1*.
(9) Hofmeier, H.; Schubert, U. S. *Chem. Soc. Rev.* **2004**, *33*, 373.
(10) Hayami, S.; Shigeyoshi, Y.; Akita, M.; Inoue, K.; Kato, K.; Osaka, K.; Takata, M.; Kawajiri, R.; Mitani, T.; Maeda, Y. *Angew. Chem., Int. Ed.* **2005**, *44*, 4899.
(11) Indumathy, R.; Radhika, S.; Kanthimathi, M.; Weyhermuller, T.; Unni Nair, B. *J. Inorg. Biochem.* **2007**, *101*, 434.
(12) Flamigni, L.; Collin, J.-P.; Sauvage, J.-P. *Acc. Chem. Res.* **2008**, *41*, 857.
(13) Eryazici, I.; Moorefield, C. N.; Newkome, G. R. *Chem. Rev.* **2008**, *108*, 1834.
(14) Hayami, S.; Komatsu, Y.; Shimizu, T.; Kamihata, H.; Lee, Y. H. *Coord. Chem. Rev.* **2011**, *255*, 1981.
(15) Wild, A.; Winter, A.; Schlutter, F.; Schubert, U. S. *Chem. Soc. Rev.* **2011**, *40*, 1459.
(16) Funaki, T.; Funakoshi, H.; Kitao, O.; Onozawa-Komatsuzaki, N.; Kasuga, K.; Sayama, K.; Sugihara, H. *Angew. Chem., Int. Ed.* **2012**, *51*, 7528.
(17) Kaveevivitchai, N.; Chitta, R.; Zong, R.; El Ojaimi, M.; Thummel, R. P. *J. Am. Chem. Soc.* **2012**, *134*, 10721.
(18) Wu, K.-L.; Li, C.-H.; Chi, Y.; Clifford, J. N.; Cabau, L.; Palomares, E.; Cheng, Y.-M.; Pan, H.-A.; Chou, P.-T. *J. Am. Chem. Soc.* **2012**, *134*, 7488.
(19) Habib, F.; Luca, O. R.; Vieru, V.; Shiddiq, M.; Korobkov, I.; Gorelsky, S. I.; Takase, M. K.; Chibotaru, L. F.; Hill, S.; Crabtree, R. H.; Murugesu, M. *Angew. Chem., Int. Ed.* **2013**, *52*, 11290.
(20) Pal, A. K.; Hanan, G. S. *Chem. Soc. Rev.* **2014**, *43*, 6184.
(21) Goodwin, H. A. *Top. Curr. Chem.* **2004**, *234*, 23.
(22) Krivokapic, I.; Zerara, M.; Daku, M. L.; Vargas, A.; Enachescu, C.; Ambrus, C.; Tregenna-Piggott, P.; Amstutz, N.; Krausz, E.; Hauser, A. *Coord. Chem. Rev.* **2007**, *251*, 364.
(23) Nielsen, P.; Toftlund, H.; Bond, A. D.; Boas, J. F.; Pilbrow, J. R.; Hanson, G. R.; Noble, C.; Riley, M. J.; Neville, S. M.; Moubaraki, B.; Murray, K. S. *Inorg. Chem.* **2009**, *48*, 7033.
(24) Hayami, S.; Karim, M. R.; Lee, Y. H. *Eur. J. Inorg. Chem.* **2013**, 683.
(25) Miller, R. G.; Narayanaswamy, S.; Tallon, J. L.; Brooker, S. *New J. Chem.* **2014**, *38*, 1932.
(26) Goodwin, H. A. *Top. Curr. Chem.* **2004**, *233*, 59.
(27) Constable, E. C.; Baum, G.; Bill, E.; Dyson, R.; van Eldik, R.; Fenske, D.; Kaderli, S.; Morris, D.; Neubrand, A.; Neuburger, M.; Smith, D. R.; Wieghardt, K.; Zehnder, M.; Zuberbühler, A. D. *Chem.—Eur. J.* **1999**, 498.
(28) Brauchli, S. Y.; Constable, E. C.; Harris, K.; Haussinger, D.; Housecroft, C. E.; Rosel, P. J.; Zampese, J. A. *Dalton Trans.* **2010**, *39*, 10739.
(29) Constable, E. C.; Thompson, A. M. W. C. *J. Chem. Soc., Dalton Trans.* **1992**, 2947.
(30) Braterman, P. S.; Song, J. I.; Peacock, R. D. *Inorg. Chem.* **1992**, *31*, 555.
(31) Bernhard, S.; Goldsmith, J. I.; Takada, K.; Abruña, H. D. *Inorg. Chem.* **2003**, *42*, 4389.
(32) Darabantu, M.; Boully, L.; Turck, A.; Plé, N. *Tetrahedron* **2005**, *61*, 2897.
(33) Kershaw Cook, L. J.; Tuna, F.; Halcrow, M. A. *Dalton Trans.* **2013**, *42*, 2254.

DOI: 10.1021/acs.inorgchem.5b00428
Inorg. Chem. 2015, 54, 5398−5409

(34) Steel, P. J. *Coord. Chem. Rev.* **1990**, *106*, 227.
(35) Johnson, C. R.; Shepherd, R. E. *Inorg. Chem.* **1983**, *22*, 2439.
(36) England, J.; Gondhia, R.; Bigorra-Lopez, L.; Petersen, A. R.; White, A. J. P.; Britovsek, G. J. P. *Dalton Trans.* **2009**, 5319.
(37) Wu, C.-D.; Hu, A.; Zhang, L.; Lin, W. *J. Am. Chem. Soc.* **2005**, *127*, 8940.
(38) Cowan, M. G.; Brooker, S. *Dalton Trans.* **2012**, *41*, 1465.
(39) Cowan, M. G.; Olguín, J.; Narayanaswamy, S.; Tallon, J. L.; Brooker, S. *J. Am. Chem. Soc.* **2012**, *134*, 2892.
(40) Cowan, M. G.; Miller, R. G.; Brooker, S. *Dalton Trans.* **2015**, *44*, 2880.
(41) Klein, A.; Kasack, V.; Reinhardt, R.; Sixt, T.; Scheiring, T.; Zalis, S.; Fiedler, J.; Kaim, W. *J. Chem. Soc., Dalton Trans.* **1999**, 575.
(42) Hellyer, R. M.; Larsen, D. S.; Brooker, S. *Eur. J. Inorg. Chem.* **2009**, 1162.
(43) Cowan, M. G.; Miller, R. G.; Southon, P. D.; Price, J. R.; Yazaydin, O.; Lane, J. R.; Kepert, C. J.; Brooker, S. *Inorg. Chem.* **2014**, *53*, 11809.
(44) Southon, P. D.; Llu, L.; Fellows, E. A.; Price, D. J.; Halder, G. J.; Chapman, K. W.; Moubaraki, B.; Murray, K. S.; Létard, J.-F.; Kepert, C. J. *J. Am. Chem. Soc.* **2009**, *131*, 10998.
(45) Muñoz-Lara, F. J.; Gaspar, A. B.; Aravena, D.; Ruiz, E.; Muñoz, M. C.; Ohba, M.; Ohtani, R.; Kitagawa, S.; Real, J. A. *Chem. Commun.* **2012**, *48*, 4686.
(46) Schubert, U. S.; Eschbaumer, C. *Angew. Chem., Int. Ed.* **2002**, *41*, 2892.
(47) Fontana, F.; Minisci, F.; Nogueira, B. M. C.; Vismara, E. *J. Org. Chem.* **1991**, *56*, 2866.
(48) Li, L.; Sarjeant, A. A. N.; Karlin, K. D. *Inorg. Chem.* **2006**, *45*, 7160.
(49) Cowan, M. G.; Brooker, S. *Coord. Chem. Rev.* **2012**, *256*, 2944.
(50) Lavallee, D. K.; Baughman, M. D.; Phillips, M. P. *J. Am. Chem. Soc.* **1977**, *99*, 718.
(51) Figard, J. E.; Paukstelis, J. V.; Byrne, E. F.; Petersen, J. D. *J. Am. Chem. Soc.* **1977**, *99*, 8417.
(52) Kilner, C. A.; Halcrow, M. A. *Dalton Trans.* **2010**, *39*, 9008.
(53) Hayami, S.; Murata, K.; Urakami, D.; Kojima, Y.; Akita, M.; Inoue, K. *Chem. Commun.* **2008**, *48*, 6510.
(54) Allen, F. H.; Bellard, S. A.; Brice, M. D.; Cartwright, B. A.; Doubleday, A.; Higgs, H.; Hummelink, T.; Hummelink-Peters, B. G.; Kennard, O.; Motherwell, W. D. S.; Rodgers, J. R.; Watson, D. G. *Acta Crystallogr., Sect. B* **1979**, *35*, 2331.
(55) Allen, F. H. *Acta Crystallogr., Sect. B* **2002**, *58*, 380.
(56) Mooibroek, T. J.; Teat, S. J.; Massera, C.; Gamez, P.; Reedijk, J. *Cryst. Growth Des.* **2006**, *6*, 1569.
(57) Mooibroek, T. J.; Gamez, P.; Reedijk, J. *CrystEngComm* **2008**, *10*, 1501.
(58) Bondi, A. *J. Phys. Chem.* **1964**, *68*, 441.
(59) Constable, E. C.; Cargill Thompson, A. M. W. *J. Chem. Soc., Dalton Trans.* **1994**, 1409.
(60) Pavlishchuk, V. V.; Addison, A. W. *Inorg. Chim. Acta* **2000**, *298*, 97.
(61) Weber, B. *Coord. Chem. Rev.* **2009**, *253*, 2432.
(62) Weber, B.; Bauer, W.; Pfaffeneder, T.; Dîrtu, M. M.; Naik, A. D.; Rotaru, A.; Garcia, Y. *Eur. J. Inorg. Chem.* **2011**, 3193.
(63) Nowak, R.; Bauer, W.; Ossiander, T.; Weber, B. *Eur. J. Inorg. Chem.* **2013**, 975.
(64) Schweinfurth, D.; Demeshko, S.; Hohloch, S.; Steinmetz, M.; Brandenburg, J. G.; Dechert, S.; Meyer, F.; Grimme, S.; Sarkar, B. *Inorg. Chem.* **2014**, *53*, 8203.
(65) (a) Kulmaczewski, R.; Olguín, J.; Kitchen, J. A.; Feltham, H. L. C.; Jameson, G. N. L.; Tallon, J. L.; Brooker, S. *J. Am. Chem. Soc.* **2014**, *136*, 878. (b) Brooker, S. *Chem. Soc. Rev.* **2015**, DOI: 10.1039/c4cs00376d.
(66) Eddaoudi, M.; Moler, D. B.; Li, H.; Chen, B.; Reineke, T. M.; O'Keefe, M.; Yaghi, O. M. *Acc. Chem. Res.* **2001**, *34*, 319.
(67) Sheldrick, G. M. *Acta Crystallogr., Sect. A* **2008**, *A64*, 112.
(68) Sheldrick, G. M.; Schneider, T. R. *Methods Enzymol.* **1997**, *277*, 319.

DOI: 10.1021/acs.inorgchem.5b00428
Inorg. Chem. 2015, 54, 5398−5409